Shear-thinning-induced chaos in Taylor-Couette flow

Nariman Ashrafi and Roger E. Khayat*
Department of Mechanical and Materials Engineering, University of Western Ontario, London, Ontario, Canada N6A 5B9
(Received 12 April 1999)

The effect of weak shear thinning on the stability of the Taylor-Couette flow is explored for a Carreau-Bird fluid in the narrow-gap limit. The Galerkin projection method is used to derive a low-order dynamical system from the conservation of mass and momentum equations. In comparison with the Newtonian system, the present equations include additional nonlinear coupling in the velocity components through the viscosity. It is found that the critical Taylor number, corresponding to the loss of stability of the base (Couette) flow, becomes lower as the shear-thinning effect increases. That is, shear thinning tends to precipitate the onset of Taylor vortex flow. Similar to Newtonian fluids, there is an exchange of stability between the Couette and Taylor vortex flows, which coincides with the onset of a supercritical bifurcation. However, unlike the Newtonian model, the Taylor vortex cellular structure loses its stability in turn as the Taylor number reaches a critical value. At this point, a Hopf bifurcation emerges, which exists only for shear-thinning fluids.

PACS number(s): 47.50.+d, 05.45.−a, 47.32.−y, 47.20.−k

I. INTRODUCTION

The interplay between inertia and shear-thinning effects is examined for axisymmetric Taylor-Couette flow (TCF) in the narrow-gap limit. Shear thinning is an inherent property of polymeric fluids used in materials processing. The rate of shearing during a polymer process can be high enough for the viscosity to change typically by a factor of 1000. It is therefore not realistic to assume that the viscosity, which is directly related to the rate of strain, be constant as in the Newtonian case. However, the presence of a rate-of-strain dependent viscosity gives rise to additional nonlinearities (in addition to inertia) and coupling among the flow variables.

Similar to any flow in the transition regime, the TCF of non-Newtonian fluids involves a continuous range of excited spatiotemporal scales. In order to assess the effect of the smaller length scales on the flow, a high resolution of the flow field is needed. It is by now well established that low-order dynamical systems can be a viable alternative to conventional numerical methods in the weakly nonlinear range of flow [1,2]. Despite the severe degree of truncation in the formulation of these models, some of the basic qualitative elements of the onset of Taylor vortices and destabilization of the cellular structure have been recovered using low-order dynamical systems.

Kuhlmann [3] and later Kuhlmann, Roth, and Lücke [4] examined the stationary and time-periodic Taylor vortex flow (TVF), in the narrow-gap limit and arbitrary gap width, respectively, with the inner cylinder rotating at a constant and harmonically modulated angular velocity. The solution to the full Navier-Stokes equations was obtained by implementing a finite-difference scheme, and an approximate approach based on the Galerkin representation. Comparison of flows based on the two methods led to good agreement. A severe truncation level was used, leading to a three-dimensional system, which turned out to be the Lorenz system with the Prandtl number equal to unity. In this case, the model cannot predict the destabilization of the Taylor vortices, and therefore cannot account for the onset of chaotic behavior.

Although dynamical systems have been mainly formulated for Newtonian fluids [3,4], they have recently been applied to non-Newtonian fluids [5–10]. Earlier formulations examined the thermal convection of viscoelastic fluids [5–7] and weakly shear-thinning fluids [8] using truncation levels similar to the Lorenz model [2]. Despite the severe level of truncation, the low-order dynamical system approach yielded a good agreement with experiments in some cases, such as the TCF of highly elastic polymeric solutions, often designated as Boger fluids [9,10].

The interplay between inertia and elasticity in TCF was first examined using a system of only six degrees of freedom [9]. The influence of higher-order modes, stemming mainly from normal stress effects, was then investigated for purely elastic fluids without inertia effects [10]. The finite amplitude elastic overstability (in the absence of inertia), which is usually observed in experiment [12], was accurately predicted for axisymmetric TVF of the Boger fluids [11] in the narrow-gap limit. The model predicts, as experiment suggests, the onset of overstability, the growth of oscillation amplitude of flow, and the emergence of higher harmonics in the power spectrum as fluid elasticity increases beyond a critical level. Also, good agreement was obtained upon comparison with the exact results from linear stability analysis [13].

In this paper, the influence of shear thinning on TVF is examined by adopting a low-order nonlinear dynamical system approach. Although the present study uses the Carreau-Bird model [11] for the viscosity dependence on the rate of strain, and thus is primarily concerned with high-molecular-weight fluids, it is also of relevance to shear-thinning fluids in general, even for some simple (monatomic) fluids. Using the method of nonequilibrium molecular dynamics, several authors [14–16] have shown that even a simple fluidlike liquid argon can exhibit rheologically complex behavior. Ashurst and Hoover [14] directly integrated the microscopic equations governing the dynamics of 108 particles. They pre-

*Author to whom correspondence should be addressed. Electronic address: rkhayat@eng.uwo.ca

dicted that the viscosity of the nonequilibrium fluid system decreases as the shear rate increases. At higher shear rate ranges, a phase transition was observed by Erpenbeck [15], which led the system to undergo a two-dimensional ordering. Heyes [16] related the rheological behavior of the flow to the dynamics of molecular interactions to investigate the cause of shear thinning in simple fluids. Based on the kinetic theory of simple dense fluids, Eu [17] and Bhattacharya and Eu [18] examined the shear-rate and frequency dependence of viscosity for a dense Lennard-Jones fluid, and compared their results with the molecular dynamics simulation of Evans [19]. Generally, the kinetic theory foundation of constitutive models for monatomic dilute (dense) simple fluids, based on the solution of the generalized Boltzmann equation, clearly reflects the non-Newtonian characteristics of such fluids [20–22]. The major distinction in constitutive behavior between these monatomic fluids and polyatomic liquids appears to be the form of transport coefficients in the limit of zero-shear-rate range [23]. The non-Newtonian character, inherent to other simple fluids such as rarefied gases, can also be inferred from the kinetic theory of Grad's 13-moment method [24].

The present study isolates the effect of shear thinning from that of fluid elasticity. The reader is referred to the review by Larson [25] for a general overview of viscoelastic instability. To our knowledge, there has been no experimental evidence of the existence of (deterministic) chaos for shear-thinning fluids similar to that for Newtonian fluids. The study, however, is not so much concerned with the emergence of shear-thinning overstability, as it focuses more on the interplay between inertia and shear thinning, and therefore on the departure from Newtonian behavior. The critical Taylor number at the onset of the Taylor vortex cellular structure is expected to be lower than that for a Newtonian fluid as a result of the decrease in viscous effects. One also expects, similar to Newtonian flow [3], that two steady-state branches emerge at the onset of a supercritical bifurcation at a critical Taylor number that depends on shear thinning. The question arises then as to whether these branches lose their stability, in turn (for instance, via a Hopf bifurcation), as the Taylor number exceeds another critical value as a result of shear thinning. This is found to be the case for the thermal convection of shear-thinning fluids [8]. Recall that the Newtonian model [3] cannot predict the destabilization of the Taylor vortex flow.

In the present paper, a level of truncation as in Refs. [3,8,9] is adopted in the Fourier representation for the flow field. Such levels of truncation have also been widely used for the Navier-Stokes and energy equations [26–28]. Examination of the influence of additional modes [29–31] indicates that many of the gross features predicted by low-order models are essentially recovered by higher-order models. The choice of a suitable constitutive model is crucial here, since the initial objective is to highlight the fundamental role shear-dependent viscosity may play in the stability of the flow.

II. PROBLEM FORMULATION

The low-order dynamical system for a Carreau fluid is derived in this section. The general equations for a weakly shear-thinning fluid are first derived in the narrow-gap limit. The three-dimensional dynamical system is then obtained using the Galerkin projection method. The coherence of the model is addressed, and a linear stability analysis is carried out involving an arbitrary number of modes to ensure the reliability of the low-order model.

A. Governing equations in the narrow-gap limit

Consider the flow of an incompressible shear-thinning fluid between two infinite, coaxial cylinders of inner and outer radii R_1 and R_2, respectively. The inner cylinder is assumed to rotate at a constant angular velocity, Ω. The outer cylinder is assumed to be at rest. In this case, the flow is governed by the following conservation of mass and linear momentum equations for an incompressible fluid:

$$\boldsymbol{\nabla}\cdot\mathbf{U}=0, \tag{1}$$

$$\rho(\mathbf{U}_{,T}+\mathbf{U}\cdot\boldsymbol{\nabla}\mathbf{U})=-\boldsymbol{\nabla}P+\boldsymbol{\nabla}\cdot(\mu\dot{\Gamma}). \tag{2}$$

where a comma denotes partial differentiation. Here $\mathbf{U}=(U_R,U_\Theta,U_Z)^T$ is the velocity vector in the cylindrical polar coordinates (R,Θ,Z), with Z taken along the common cylinder axis, P is the pressure, μ is the shear-rate dependent viscosity, ρ is the density, T is the time, $\boldsymbol{\nabla}$ is the three-dimensional gradient operator, and $\dot{\Gamma}=\boldsymbol{\nabla}\mathbf{U}+(\boldsymbol{\nabla}\mathbf{U})^T$ is the rate-of-strain tensor. The fluid is assumed to have a zero-shear-rate viscosity μ_0. In this study, only axisymmetric flow is considered, so that the dependence on Θ is neglected.

The first step in reducing Eqs. (1) and (2) to the narrow-gap limit consists of introducing dimensionless coordinates, x and z, in the transverse and axial directions, respectively, time t, pressure p, velocity components u_x, u_y, and u_z, and viscosity η, as follows:

$$x=\frac{R-R_1}{D},\quad z=\frac{Z}{D},\quad t=\frac{\nu_0}{D^2}T,\quad p=\frac{D^2}{\rho\nu_0^2}P,$$

$$u_x=\frac{D}{\nu_0}U_R,\quad u_y=\frac{1}{R_1\Omega}U_\Theta,\quad u_z=\frac{D}{\nu_0}U_Z,\quad \eta=\frac{\mu}{\mu_0}, \tag{3}$$

where $D=R_2-R_1$ is the gapwidth, and $\nu_0=\mu_0/\rho$ is the zero-shear-rate kinematic viscosity.

In this study, the flow is taken as the superposition of the base flow and a perturbation from the base flow. Unlike Newtonian flow, Eq. (2) can admit a multiplicity of steady-state solutions because of the nonlinearity resulting from shear thinning. In the narrow-gap limit (see below), the steady pressure, p^0; and transverse velocity component, u_y^0, are governed by

$$p_{,x}^0=\mathrm{Ta}(u_y^0)^2,\quad \frac{d}{dx}\left[\eta\left(\frac{du_y^0}{dx}\right)\frac{du_y^0}{dx}\right]=0, \tag{4}$$

where the dependence of the viscosity, η, on the shear rate is shown implicitly. Here Ta is the Taylor number, which will be introduced shortly. While the pressure is uniquely given in terms of the velocity, there may be more than one solution for the latter. The purely azimuthal or circular Couette flow (CCF) is only one possible solution. In other words, setting

the shear rate to constant after integrating the second equation in Eq. (4) is one among many possibilities. Other possibilities include a shear rate that is y dependent but such that the product of viscosity and shear rate remains constant. It is anticipated that the CCF solution loses its stability once the Taylor number exceeds a critical level. However, the question arises, given the multiplicity of the steady-state solution, as to whether the CCF is the most stable solution in the precritical range of Taylor numbers. This question will only be addressed briefly below. In this work, the CCF is the only base flow whose stability is examined. In the narrow-gap limit, the corresponding velocity components $(u_x^0,u_y^0,u_z^0)^T$ and pressure p^0, are given explicitly as

$$u_x^0=u_z^0=0, \quad u_y^0=1-x, \quad p,_x^0=\mathrm{Ta}(1-x)^2, \tag{5}$$

in which Ta is defined in terms of the Reynolds number, Re, and the gap-to-radius ratio, ε:

$$\mathrm{Ta}=\mathrm{Re}^2\,\varepsilon; \quad \mathrm{Re}=\frac{\Omega R_1 D}{\nu_0}, \quad \varepsilon=\frac{D}{R_1}, \tag{6}$$

It is important to observe that the CCF in Eq. (5) is independent of the form of the viscosity since the shear rate is constant.

In this work, the Carreau-Bird model is adopted, more particularly for weakly shear-thinning fluids (with small time constant). A major advantage of this model over other models, such as the power-law model, is that Newton's law of viscosity [11] is recovered in the limit of zero shear rate [3]. The general Carreau-Bird viscosity model can be written in dimensionless form:

$$\eta(\dot\gamma)=s+(1-s)[1+(\mathrm{De}\,\dot\gamma)^2]^{(n-1)/2}, \tag{7}$$

where n is the ''power-law exponent,'' which is less than 1 for shear-thinning fluids, $\dot\gamma$ is the magnitude of the dimensionless rate-of-strain tensor $\dot\gamma=(D/R_1\Omega)\dot\Gamma$, and s is the ratio of the zero to infinite shear-rate viscosities [11]. Here, $\mathrm{De}=\lambda R_1\Omega/D$ is the ''Deborah number'' for the problem, λ being the time constant. More explicitly, $\dot\gamma$ is expressed in terms of the components of the rate-of-strain tensor, $\dot\gamma$, as [11]

$$\dot\gamma=\sqrt{\dot\gamma_{xy}^2+\dot\gamma_{xz}^2+\dot\gamma_{yz}^2+\frac{\varepsilon}{2\,\mathrm{Ta}}(\dot\gamma_{xx}^2+\dot\gamma_{yy}^2+\dot\gamma_{zz}^2)}, \tag{8}$$

where it is recalled that $\dot\gamma_{ij}=u_{i,j}+u_{j,i}$, with $i,j=x,y,z$. Note that in the present problem, $\dot\gamma_{yy}^2=0$ since the flow is axisymmetric and the gap between the two cylinders is narrow. In this study, it is assumed that $\mathrm{Ta}=O(1)$, so that the terms of $O(\varepsilon/\mathrm{Ta})$ in Eq. (8) can be neglected. If De is small, then η may be reduced to

$$\eta(\dot\gamma)=1+(1-s)\left(\frac{n-1}{2}\right)(\mathrm{De}\,\dot\gamma)^2=1+\alpha\dot\gamma^2, \tag{9}$$

where higher-order terms in De have been neglected, and $\alpha=(1-s)(n-1/2)\mathrm{De}^2$.

Hereafter in this paper, the parameter α is used as a measure of non-Newtonian effect, and is assumed to be small enough for approximation (8) to hold. Thus, in the limit $\alpha\to0$, one recovers the expression for the Newtonian viscosity. It should be noted that α is negative (positive) for shear-thinning (thickening) fluids. It is thus assumed $|\alpha|\ll1$. Note that expression (9) also corresponds to second-order fluids [11].

The deviation from the CCF, u_x', u_y', and u_z', for the velocity components, p' for the pressure, and η' for the viscosity, are defined as

$$u_x'=u_x-u_x^0, \quad u_y'=u_y-u_y^0, \quad u_z'=u_z-u_z^0,$$
$$p'=p-p^0, \qquad \eta'=\eta-\eta^0. \tag{10}$$

The explicit expressions for η^0 and η' will be given shortly. Using Eqs. (3), (5), (9), and neglecting terms of $O(\varepsilon)$, Eqs. (1) and (2) reduce to the following form in the narrow-gap limit:

$$u_{x,x}+u_{z,z}=0 \tag{11a}$$

$$u_{x,t}+u_xu_{x,x}+u_zu_{x,z}-\tau_y^2-2\tau_y(1-x)=-p_{,x}+(\eta^0+\eta)(u_{x,xx}+u_{x,zz})+2\eta_{,x}u_{x,x}+\eta_{,z}(u_{x,z}+u_{z,x}), \tag{11b}$$

$$u_{y,t}+u_xu_{y,x}+u_zu_{y,z}=u_x+(\eta^0\eta)(u_{y,xx}+u_{y,zz})+\eta_{,z}u_{y,z}+\eta_{,x}(u_{y,x}-1), \tag{11c}$$

$$u_{z,t}+u_xu_{z,x}+u_zu_{z,z}=-p_{,z}+(\eta^0+\eta)(u_{z,xx}+u_{z,zz})+2\eta_{,z}u_{z,z}+\eta_{,x}+(u_{x,z}+u_{z,x}), \tag{11d}$$

where, for simplicity, the primes are dropped. Finally, by substituting for $\dot\gamma$, we obtain the expressions for η^0 and η (or η').

$$\eta^0=1+\alpha, \qquad \eta=\alpha(u_{y,x}^2+u_{y,z}^2-2u_{y,x}). \tag{12}$$

The solution of Eqs. (11) is considered next using the method of Galerkin projection.

B. Galerkin projection and the dynamical system

The Galerkin projection method consists of expanding the velocity and pressure in terms of orthogonal functions of x and z, and project Eqs. (11) onto each mode of expansion to generate a set of ordinary differential equation that govern the time-dependent expansion coefficients. The type of orthogonal functions depends on the geometry and boundary conditions. A periodic solution is taken along the cylinder axis. For simplicity, the rigid-free boundary conditions are assumed. The fluid is assumed to adhere to the cylinders in the azimuthal direction, and it is assumed to slip along the z direction.

We follow Kuhlmann and co-workers [3,4] to obtain the flow departure by solving Eqs. (11) and introducing infinite Fourier series in the x and the z directions, with the series coefficients depending only on time. The general solution for the axisymmetric TVF can be decomposed into sine and cosine normal modes as

TABLE I. Influence of higher-order modes on the values of the critical Taylor number, Ta_c^m and corresponding wave number, k_m. Here $\alpha=-1$.

	Newtonian fluid		Shear-thinning fluid	
Number of modes	k_m	Ta_c^m	k_m	Ta_c^m
1	2.221 40	657.511 36	2.127 90	452.557 79
2	2.227 20	654.256 57	2.130 60	451.554 32
3	2.227 20	654.256 50	2.130 60	451.554 31
4	2.227 20	654.256 09	2.130 60	451.554 19
5	2.227 20	654.256 09	2.130 60	451.554 19
10	2.227 20	654.256 09	2.130 60	451.554 19

$$u_x(x,z,t)=\sum_{n=1}^{\infty}\sum_{m=1}^{\infty}\hat{u}_{nm}(t)\sin n\pi x\cos mkz, \quad (13a)$$

$$u_y(x,z,t)=\sum_{n=1}^{\infty}\left[\sum_{m=1}^{\infty}\hat{v}_{nm}(t)\sin n\pi x\cos mkz+\hat{v}_{n0}(t)\sin n\pi x\right], \quad (13b)$$

$$u_z(x,z,t)=\sum_{n=1}^{\infty}\sum_{m=1}^{\infty}\hat{w}_{nm}(t)\cos n\pi x\sin mkz, \quad (13c)$$

$$p'(x,z,t)=\sum_{n=1}^{\infty}\sum_{m=1}^{\infty}\hat{p}_{nm}(t)\cos n\pi x\cos mkz, \quad (13d)$$

where $\hat{u}_{nm}(t)$, $\hat{v}_{nm}(t)$, $\hat{w}_{nm}(t)$, and $\hat{p}_{nm}(t)$ are time-dependent coefficients and k is the dimensionless wave number in the z direction. The first step in the Galerkin projection method consists of substituting Eqs. (13) into Eqs. (11). Equations (11) are then multiplied by the appropriate mode and are integrated over $x\in[0,1]$ and $z\in[0,\pi/k]$.

The basic model, which involves only dominant modes, consists of the fundamental modes $\hat{u}_{11}(t)$, $\hat{v}_{11}(t)$, $\hat{w}_{11}(t)$, and $\hat{p}_{11}(t)$, which are coupled nonlinearly by $\hat{v}_{10}(t)$ and $\hat{v}_{20}(t)$. The justification for such a severe level of truncation is based on the results from linear stability analysis (see below). Comparison between exact and approximate values for the critical Taylor and wave numbers leads to excellent agreement.

After eliminating the pressure coefficient, the resulting set of nonlinear and coupled ordinary differential equations, which govern the time-dependent expansion coefficients, become

$$\frac{d\hat{u}_{11}}{dt}=\tau k^2\mathrm{Ta}\hat{v}_{11}-\tau^{-1}\hat{u}_{11}+\mathrm{Ta}\frac{16\tau k^2}{3\pi}\hat{v}_{11}\hat{v}_{10}+\alpha(A_1\hat{v}_{11}^2\hat{u}_{11}+A_2\hat{v}_{10}^2\hat{u}_{11}+A_3\hat{v}_{20}^2\hat{u}_{11}+A_4\hat{v}_{20}\hat{u}_{11}+A_5\hat{u}_{11}), \quad (14a)$$

$$\frac{d\hat{v}_{11}}{dt}=\pi\hat{u}_{11}\hat{v}_{20}+\hat{u}_{11}-\tau^{-1}\hat{v}_{11}+\alpha(B_1\hat{v}_{11}^3+B_2\hat{v}_{10}^2\hat{v}_{11}+B_3\hat{v}_{20}^2\hat{u}_{11}+B_4\hat{v}_{20}\hat{v}_{11}+B_5\hat{v}_{11}), \quad (14b)$$

$$\frac{d\hat{v}_{20}}{dt}=-\frac{\pi}{2}\hat{u}_{11}\hat{v}_{11}-4\pi^2\hat{v}_{20}+\alpha(C_1\hat{v}_{20}^3+C_2\hat{v}_{11}^2\hat{v}_{20}+C_3\hat{v}_{10}^2\hat{v}_{20}+C_4\hat{v}_{11}^2+C_5\hat{v}_{10}^2+C_6\hat{v}_{20}), \quad (14c)$$

$$\frac{d\hat{v}_{10}}{dt}=-\pi^2\hat{v}_{10}+\alpha(D_1\hat{v}_{10}^3+D_2\hat{v}_{11}^2\hat{v}_{10}+D_3\hat{v}_{20}^2\hat{v}_{10}+D_4\hat{v}_{20}\hat{v}_{10}+D_5\hat{v}_{10}), \quad (14d)$$

where $A_1,\ldots,A_5$, $B_1,\ldots,B_5$, $C_1,\ldots,C_6$, $D_1,\ldots,D_5$, depend only on k and are given in Appendix A. Here $\tau=(1/\pi^2+k^2)$. Note that we made use of the relation $\hat{w}_{11}(t)=-(\pi/k)\hat{u}_{11}(t)$, which results from the continuity equation.

In order to justify the restricted number of modes in the x direction, the minimum critical Taylor number, Ta_c^m, and corresponding wave number, k_m, are first computed using an arbitrary number of modes, N. The details of the derivation are given in Appendix B. The linear stability analysis of Eqs. (11) is carried out using the general solution (13) with $N=1$. The influence of the number of eigenmodes in the x direction is reflected in Table I for both a Newtonian fluid and a shear-thinning fluid with $\alpha=-0.1$. The table indicates that the higher-order modes cause corrections to the first approximation that are of order 10^{-2} for both fluids. The comparison thus shows that the severe truncation level adopted in the current study is not unreasonable.

The set of Eqs. (14) is reduced to a three-dimensional system if we note that $\hat{v}_{10}(t)$ can be decoupled from the remaining coefficients. This is demonstrated by first rewriting Eq. (14d) compactly as

$$\frac{d\hat{v}_{10}}{dt}=[-\pi^2+\alpha F(\hat{v}_{10},\hat{u}_{11},\hat{v}_{11},\hat{v}_{20})]\hat{v}_{10}. \quad (15)$$

Since α is considered to be small ($-0.1<\alpha<0$) and F is $O(1)$, the term $-\pi^2+\alpha F$ is $O(\pi^2)$ and the contribution of αF is negligible. This means that $\hat{v}_{10}(t)$ decays exponentially with time, with uninteresting transients, similarly to the Newtonian case ($\alpha=0$). Therefore, with the following scaling for the most prominent modes

$$u=\frac{\pi\tau}{\sqrt{2}}\hat{u}_{11}(t), \quad v=\frac{\pi}{\sqrt{2}}\hat{v}_{11}(t), \quad w=-\pi\hat{v}_{20}(t), \quad (16)$$

we finally arrive at the following three-dimensional dynamical system:

$$\dot{u}=r\nu-u-\frac{\alpha}{2}\left\{\left[(4-b)(b-2)+\frac{9}{b}-2\right]u\nu^2+2(2-b)uw^2 -(b-2)^2-(b-2)^2uw+2u\right\}, \tag{17a}$$

$$\dot{\nu}=-uw+u-\nu-\frac{\alpha}{2}\left\{\left[\frac{9}{b}+b-4\right]\nu^3+2(b+2)\nu w^2 -2(b-2)\nu w+(b+2)\nu\right\}, \tag{17b}$$

$$\dot{w}=u\nu-bw-\frac{\alpha}{2}[6bw^3+2(b+2)\nu^2w+(b+2)\nu^2+6bw], \tag{17c}$$

where a dot denotes total differentiation with respect to time, and $b=4\pi^2\tau$. For convenience here, we have introduced the reduced Taylor number, r, which will be used later as a control parameter for the stability analysis:

$$r=\mathrm{Ta}\tau^3k^2. \tag{18}$$

The analysis of the solution of Eqs. (17) is our main objective. In the limit $\alpha\to0$, Eqs. (17) reduce to the Newtonian form [3], which corresponds to the Lorentz system with the Prandtl number set equal to 1 [32]. Compared to the Newtonian system, Eqs. (17) are highly nonlinear. In addition to the usual nonlinearities stemming from inertia effects, there are nonlinearities stemming from shear-thinning effects. Finally, we note that Eqs. (17) are invariant under the symmetry operation $(u,\nu,w)\to(-u,-\nu,w)$. This is consistent with the physical situation of shear-thinning fluids and the orientation of the flow within the vortex structure.

C. Consistence of the low-order model

As in the case of the Newtonian system, it should be ensured that the introduction of the severe truncation has not caused a singularity in the lower-order model (17), and that the model remains physically consistent. To this end, we use a Lyapunov function for the model and show that the solution of Eqs. (17) remains bounded [33]. In other words, we must show that the three-dimensional field (u, ν, w) is everywhere directed toward the origin on a surface surrounding the origin, and is located at a large distance from it. Let $F(u,\nu,w)=0$ be the equation of such a surface. Thus, we must have, everywhere in phase space:

$$DF=\dot{u}F_{,u}+\dot{\nu}F_{,\nu}+\dot{w}F_{,w}<0. \tag{19}$$

There is a wide range of possibilities for the choice of the surface F. The following sphere turned out to be a suitable choice:

$$F(u,\nu,w)=\frac{1}{2}(u^2+\nu^2+w^2)-A, \tag{20}$$

with $A>0$ and arbitrarily large. Substituting this expression for F into Eq. (19), and using Eqs. (17), to obtain

$$DF=-u^2-\nu^2-bw^2+(r+1)u\nu+\alpha G(u,\nu,w), \tag{21}$$

where $G(u,\nu,w)$ is an explicit polynomial function of u, ν, and w. It is evident that for values of $|\alpha|\ll1$, terms multiplied by α in Eq. (21) are dominated by the quadratic terms, and therefore, DF remains negative. In this case, no trajectory originating from a point with a finite distance from the origin can go off to infinity. Thus, the basin of attraction around the origin becomes larger for smaller values of α.

We now turn our attention to the coherence of the model pertaining to the volume contraction. Consistently with the original equation (1), Eqs. (17) must be dissipative. Thus, a volume, $V(t)$, in phase space must contract. For volume contraction to be insured, the velocity field must have a constant negative divergence everywhere or

$$\frac{1}{V(t)}\frac{dV(t)}{dt}=\frac{\partial\dot{u}}{\partial u}+\frac{\partial\dot{\nu}}{\partial\nu}+\frac{\partial\dot{w}}{\partial w}=-2-b+\alpha H(u,\nu,\psi). \tag{22}$$

Here H is a polynomial in u, ν, and w, which is not given explicitly. From the expression above, we note that for $|\alpha|\ll1$, $V^{-1}dV/dt$ becomes approximately equal to a constant: $-(2+b)$, i.e., the volume decreases monotonically with time.

III. BIFURCATION AND STABILITY ANALYSIS

In this section, we obtain the steady-state solution(s) of Eqs. (17). Some of these solution branches correspond to purely circular (Couette) flow, and other branches correspond to toroidal (Taylor-vortex) flow. The stability of both the CCF and TVF is examined by exploring some of the fundamental differences between Newtonian and shear-thinning fluids. In comparison with the Newtonian system, the presence of the nonlinear terms resulting from shear thinning leads to additional complexity from both the mathematical and physical points of view. Expectedly, for very small values of α, similar behavior is obtained for Newtonian and non-Newtonian fluids.

A. Stability of the base flow

The stability analysis for a shear-thinning fluid is carried out around the CCF (origin in phase space). The analysis is based on the linearization of Eqs. (17), and is similar to the analysis based on the Newtonian equations [3]. Linear stability analysis around the origin leads to three characteristic roots, one root $\lambda_1=-b(1+3\alpha)$, turns out to be independent of r, and the other two roots are governed by the following equation:

$$\lambda^2+\left[2(1+\alpha)-\frac{\alpha b}{2}\right]\lambda+(r_c-r)=0. \tag{23}$$

Thus, λ_1 is positive for $\alpha>-1/3$. With the assumption of fluid being weakly shear thinning, α cannot reach this value. The other two roots, λ_2 and λ_3, are always real. One of the roots, λ_2, is always negative, and λ_3 becomes positive for $r>r_c$, with r_c given by

$$r_c=(1+\alpha)^2+(1+\alpha)\alpha b/2. \tag{24}$$

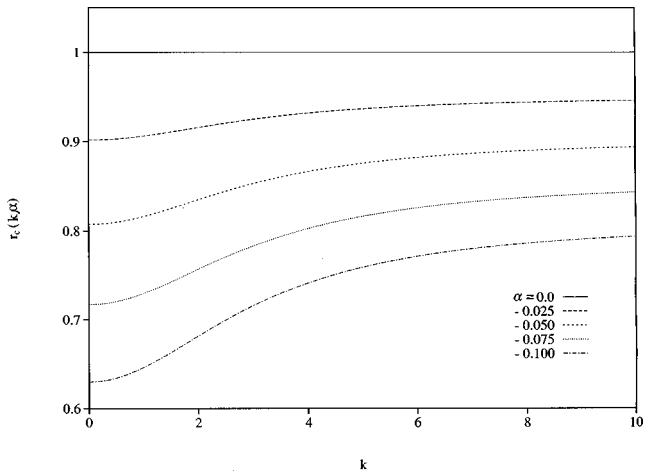

FIG. 1. Influence of shear thinning on the onset of Taylor vortex flow. Critical value $r=r_c$ at the onset of supercritical bifurcation (Taylor vortex flow) as function of k for $-0.1\leqslant\alpha\leqslant 0$.

Note that for a Newtonian fluid, $r_c=1$. The second term in this expression contributes to the decrease of r_c similarly to the first term, as α assumes smaller values (note that $\alpha<0$). The effect of the second term, however, is not as significant as that of the first one. The dependence of r_c on the wave number k is depicted in Fig. 1 for typical values of α. It is evident from the figure that for smaller α values, in the range $0<k<4$, r_c increases noticeably, while for $k>4$ this increase is insignificant. This explains why, for a given α in the range $k>4$, the stability analysis around the origin gives almost the same results regardless of value of k. However, as α increases, r_c becomes less sensitive to changes in k.

It is instructive to explore the variations of the critical Taylor number $\mathrm{Ta}_c=r_c/\tau^3k^2$ as a function of k. For a given α value, the minimum critical Taylor number, Ta_c^m, occurs at a wave number $k_m=\pi\sqrt{(\alpha+1)/(\alpha+2)}$. For $\alpha\in[-0.1,0.0]$, k_m decreases monotonically as with shear thinning at most only 3% from the critical wave number for the Newtonian case $(\pi/\sqrt{2})$ [3]. Figure 2 shows the behavior of the critical Taylor number as a function of the wave number for typical values of α. For all α values, Ta_c decreases like

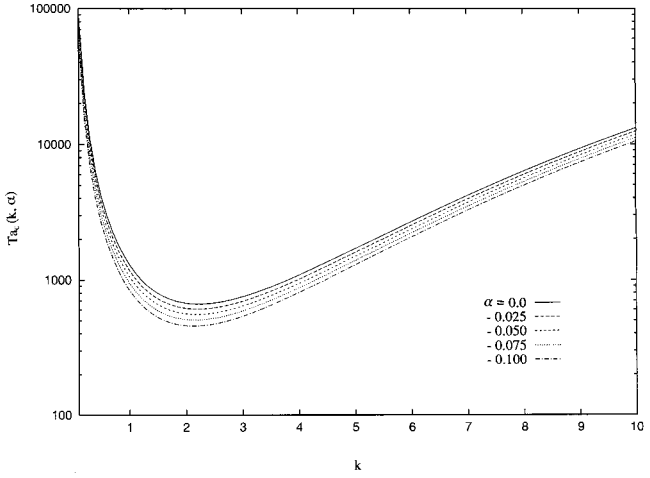

FIG. 2. Influence of shear thinning on marginal stability curves. Variation of the critical Taylor number, Ta_c, as function of k for $-0.1\leqslant\alpha\leqslant 0$.

$1/k^2$ near $k=0$, reaches a minimum, and then increases like k^2 for large k's. The value of k_m tends to increase as α decreases. On the other hand, this minimum becomes less pronounced with increasing shear thinning of the fluid, resulting in a wider range of Taylor vortices near Ta_c^m. It is inferred from Fig. 2 that shear thinning tends to precipitate the onset of axisymmetric Taylor vortices at any value of the wave number in the axial direction. As shear thinning increases, the critical Taylor number reaches a zero value [$\alpha=-1$ in Eq. (24)]. In this case, we formally recover the Rayleigh stability picture for an inviscid fluid. The recovery of the limit of zero critical Taylor number must of course be interpreted with caution as the limit $\alpha=-1$ is not within the range of validity of the present theory.

B. Steady-state solutions and bifurcation diagrams

As in the Newtonian equations, a trivial solution of Eqs. (17) exists, which corresponds to the CCF or the origin in phase space:

$$u_s(r,\alpha)=\nu_s(r,\alpha)=w_s(r,\alpha)=0. \tag{25}$$

In the limit $\alpha\to 0$, the nontrivial steady-state solution branches for a Newtonian fluid are given by

$$u_s^N(r)=\pm\sqrt{b(r-1)},\quad \nu_s^N(r)=\pm\frac{\sqrt{b(r-1)}}{r},$$

$$w_s^N(r)=\frac{r-1}{r}. \tag{26}$$

For shear-thinning fluids, similar nontrivial, steady-state solution branches exist, but they cannot be obtained analytically. These two sets of branches will be denoted by C_1 and C_2. In order to determine the steady-state branches of u, ν, and w in Eqs. (17), a modified Newton-Raphson method is used (IMSL-DNEQNJ), with the Jacobian of the system being provided. However, despite the robustness of the Newton-Raphson method, and the fact that the nonlinearities involved in the algebraic equations are only polynomials, the bifurcation branches for various α values were found to be difficult to generate. The steady-state solution was found to be extremely sensitive to the initial guess. The guess had to be provided accurately enough for the method to converge. This difficulty was circumvented by transforming the algebraic equations for $u_s(r,\alpha)$, $\nu_s(r,\alpha)$, and $w_s(r,\alpha)$ into a set of ordinary differential equations, with r being the independent variable. The set of three algebraic equations are, of course, obtained by setting the time derivative in Eqs. (17) equal to zero. Three first order differential equations are obtained by differentiating the algebraic equations with respect to r. This strategy is now illustrated in the case of a Newtonian fluid, although an analytical solution exists in this case. The algebraic equations that govern the Newtonian steady-state flow are

$$r\nu_s^N-u_s^N=0,\quad -u_s^Nw_s^N+u_s^N-\nu_s^N=0,\quad u_s^N\nu_s^N-bw_s^N=0. \tag{27}$$

If the solution to this set of equations is sought for a given r value, then the steady-state solution can be considered as the

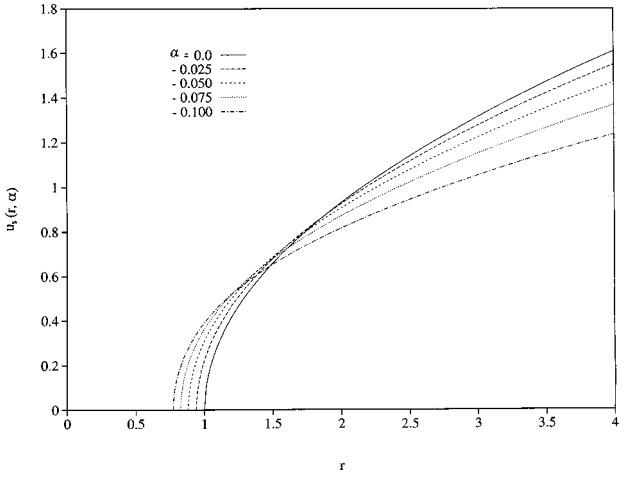

FIG. 3. Influence of shear thinning on TVF. Bifurcation diagrams for $u=u_s$ as function of r for $-0.1\leqslant\alpha\leqslant 0$ $(k=6)$. Note that only one branch is shown (C_1 and not C_2) because of symmetry.

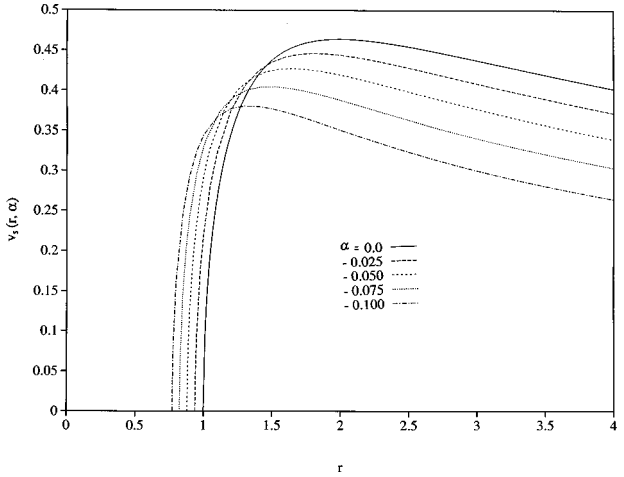

FIG. 4. Influence of shear thinning on TVF. Bifurcation diagrams for $\nu=\nu_s$ as function of r for $-0.1\leqslant\alpha\leqslant 0$ $(k=6)$.

dependent variable, and r becomes the independent variable. Then the differential equations are obtained by differentiating the system of three equations above with respect to r, to give

$$\frac{du_s^N}{dr}=\frac{r\lfloor u_s^N\nu_s^N+b(w_s^N-1)\rfloor\nu_s^N}{b(r-1-rw_s^N)-ru_s^N\nu_s^N-{u_s^N}^2}+\nu_s^N, \tag{28a}$$

$$\frac{d\nu_s^N}{dr}=\frac{\lfloor u_s^N\nu_s^N+b(w_s^N-1)\rfloor\nu_s^N}{b(r-1-rw_s^N)-ru_s^N\nu_s^N-{u_s^N}^2}, \tag{28b}$$

$$\frac{dw_s^N}{dr}=\frac{[u_s^N\nu_s^N+b(w_s^N-1)](r\nu_s^N+u_s^N)\nu_s^N}{r-1-rw_s^N-b(r\nu_s^N+u_s^N)u_s^N}+\frac{{\nu_s^N}^2}{b}. \tag{28c}$$

Thus, for a shear-thinning fluid, a solution branch is sought, for a given α, by first seeking a solution point provided by the Newton-Raphson method. Then using this point as an ''initial'' value, the solution branch is generated using a sixth-order Runge-Kutta algorithm (IMSL-DIVERK). Note that the starting point (obtained using the Newton-Raphson method) at $r=r_{ini}$, is usually difficult to obtain near the critical point, and it is typically evaluated far ahead, for $r_{ini}>r_c$. The nontrivial solution branch is then generated (using the Runge-Kutta method) by increasing r, for the range $r>r_{ini}$, and then by decreasing r for the range $r_c<r<r_{ini}$. However, it is important to note that Eqs. (28) are also difficult to solve near the critical point as they become singular at $r=r_c$.

The steady-state branches u_s, ν_s, and w_s for $\alpha\in[-0.1,0.0]$ and $k=6$ are plotted as functions of r, and are shown in Figs. 3, 4, and 5, respectively. This value of the wave number is chosen for clarity (see below). It can be seen from Fig. 3 that, in general, the origin (in phase space) remains the only steady-state solution of Eqs. (17) until r reaches a critical value, r_c, which is equal to one for the Newtonian case [see Eqs. (26)]. At this point, two additional fixed branches, C_1 and C_2, emerge, which correspond to the onset of Taylor vortices. More specifically, a supercritical bifurcation is observed at the critical point. Since each bifurcation diagram is symmetric, only one set of solution branches (C_1) is shown. As α decreases from zero, r_c takes on lower values. Shear thinning tends to accelerate the flow in the (x,z) plane near the onset of TVF. For the higher range of r values, shear thinning tends to slow the flow down. Regarding the (deviation) flow in the azimuthal direction, similar observations apply to $\nu_s(r,\alpha)$, which is related to $\hat{\nu}_{11}(t)$ (Fig. 4). However, $w_s(r,\alpha)$, which is related to $\hat{\nu}_{20}(t)$, increases with both inertia and shear thinning monotonically (Fig. 5).

Two additional nontrivial steady-state solution branches were also identified, which do not exist for a Newtonian fluid. These solutions are independent of r, and exist only if $-1/6<\alpha<0$ for a shear-thinning fluid. The solution branches are given by $u_s(r,\alpha)=\nu_s(r,\alpha)=0$ and $w_s(\alpha)=\pm[-(1+3\alpha)/3\alpha]^{1/2}$. They represent approximations to nonlinear purely swirling flows, in addition to the CCF. Whether these flow profiles have any physical significance is difficult to assert, especially for purely shear-thinning fluids. For some flows that obey nonaffine viscoelastic constitutive

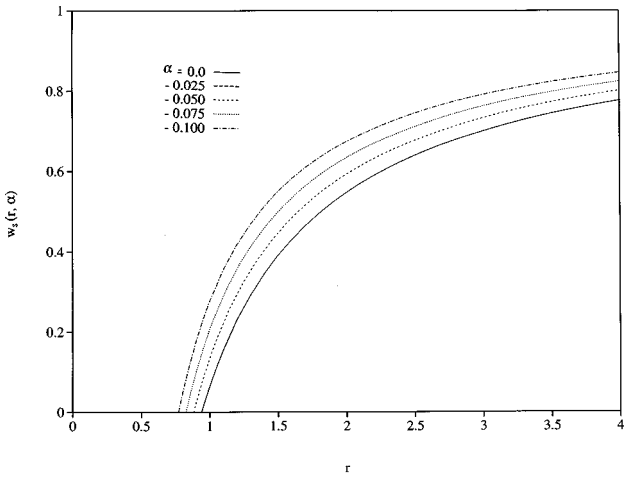

FIG. 5. Influence of shear thinning on TVF. Bifurcation diagrams for $w=w_s$ as function of r for $-0.1\leqslant\alpha\leqslant 0$ $(k=6)$. Note the two additional steady-state branches $w_s(\alpha)=\pm[-(1+3\alpha)/3\alpha]^{1/2}$ are not shown.

equations (also exhibiting shear-thinning effects), similar nonlinear (Couette) flow profiles are obtained [34]. The two additional branches are an example of the solution multiplicity of Eq. (4). However, they can also be an artifact resulting from the severe truncation used, but may be more or less stable than the CCF. The analysis of stability of these two branches will not be addressed in the current paper.

C. Stability of the Taylor vortex flow

Consider next the stability of the steady-state branches C_1 and C_2 as r is increased beyond r_c. For a Newtonian fluid, linearization of Eqs. (17) around the steady-state branches (26) leads to the following characteristic equation:

$$\lambda^3+(b+2)\lambda^2+b(r+1)\lambda+2b(r-1)=0. \qquad (29)$$

The roots of Eq. (29) have a real part that remains negative for any value of r. Thus, for $r>r_c$, the three-dimensional Newtonian model cannot predict any destabilization of the TVF.

Linear stability analysis around the C_1 and C_2 branches for a shear-thinning fluid leads to a cubic characteristic equation similar to Eq. (29). However, the coefficients in this case are not explicitly expressible in terms of the steady-state solutions; these latter not being available analytically. In this case, the coefficients of the λ terms in the characteristic equation are determined numerically. Computations show that these branches are linearly stable for $r>r_c$ near r_c. In a typical case of $\alpha=-0.075$ and $k=6$, the linear stability is lost to an inverse Hopf bifurcation at $r_{hl}=34.8$. At this point, only an aperiodic solution exists in the form of a strange attractor [2]. This situation holds as long as α remains close to zero. The bifurcation picture is therefore shown schematically in Fig. 6. At some point $r_{h2}=12.5$, the inverse Hopf bifurcation branches intersect the r axis. Here, in the range $r\in[1,12.5]$, C_1 and C_2 are globally stable; for any initial perturbation, the solution converges to these branches (see Fig. 6). In the range $r\in[12.5,34.8]$, the solutions will converge to C_1 and C_2 only if the initial perturbation is not too large; the branches are locally stable. In this range, if the perturbation is too large, a chaotic solution results. Thus, r_{h2} is determined numerically, and it corresponds to the point where C_1 and C_2 lose their global (to only local) stability. Note that the dashed lines illustrating the amplitude of the inverse bifurcation in the Fig. 6 are only sketched and not accurately determined. Beyond $r=34.8$, stability is not achieved although there is some order within the chaos via inverse period doubling and intermittency.

Variation of r_{h1} vs k for the range $\alpha\in[-0.07,-0.1]$ is depicted in Fig. 7. It can be observed that r_{h1} for $-0.07<\alpha<-0.08$ is very sensitive to the choice of α. In this range, r_{h1} increases sharply with k. At about $\alpha=-0.075$, r_{h1} changes curvature and levels off at some higher k value. This trend continues until no substantial change for the case $\alpha=-0.1$ is detected. Thus, the TVF appears to be always unstable for pronounced shear thinning.

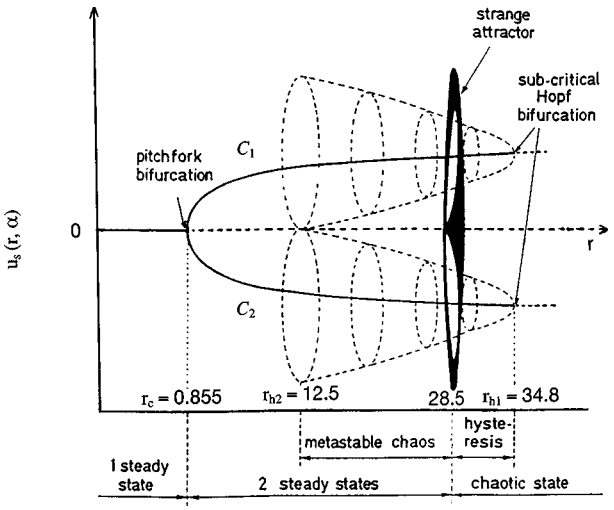

FIG. 6. Schematic illustration giving the overall stability and bifurcation picture for a shear-thinning fluid for $\alpha=-0.075$ and $k=6$. The supercritical pitchfork bifurcation (with branches C_1 and C_2) emerges at $r_c=0.855$. The subcritical Hopf bifurcation emerges at $r_{h1}=34.8$, and intersects the r axis at $r_{h2}=12.5$. Stable and unstable branches are drawn using solid and dashed lines, respectively. Note that the notations used in the figure and figure layout are the same as those corresponding to the Lorenz system in Ref. [2].

IV. NONLINEAR DYNAMICAL BEHAVIOR

While the analysis above determines the conditions for instability of the steady-state branches, the full nonlinear behavior can only be understood when the numerical solution of Eqs. (17) is obtained. The time-dependent evolution of flow is carried out using a sixth-order Runge-Kutta scheme (IMSL-DIVERK). The solution depends on the initial conditions assumed. It is found that, regardless of these conditions the long-term behavior will be essentially the same after transients die out, indicating that the solution branch is unique, at least for the range of parameters covered.

The present calculations are conducted for a fluid with $\alpha=-0.075$ and $k=6$, corresponding to a typical Carreau-Bird fluid. The choice of these parameters is not entirely arbitrary. This choice turns out to be appropriate as interesting dynamics are observed when r is varied. In particular,

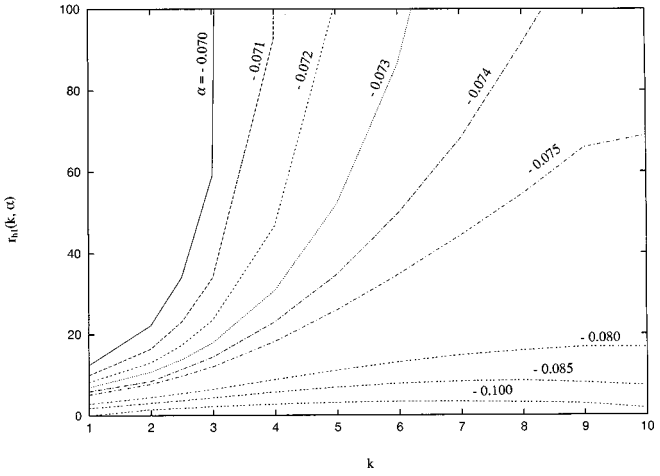

FIG. 7. Influence of shear thinning on the destabilization of the Taylor vortex flow. Critical point $r=r_{h1}$ vs k at the onset of the subcritical Hopf bifurcation for $-0.1\leqslant\alpha\leqslant-0.07$. Note that $\lim_{\alpha\to 0} r_{h1}(r,\alpha)\to\infty$.

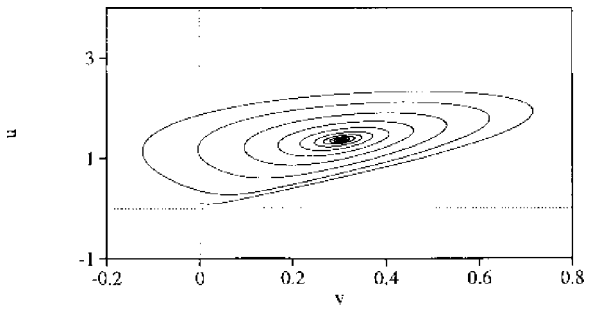

FIG. 8. Time decaying flow. Phase trajectory in the (u,v) plane for $r=4$, $\alpha=-0.075$, and $k=6$.

and on the basis of Fig. 2, a more appropriate value for the wave number would be 2.2, as it is roughly at this value that the first instability is likely to be observed. However, the dynamics based on $k=2.2$ is similar but more difficult to clearly observe than that based on $k=6$. In what follows, the influence of inertia for a shear-thinning fluid is examined by varying r. We choose to represent the various solutions as time signatures, phase plots, and/or power spectra depending on which of these representations is most insightful.

A. Onset of early chaos

Consider the range of r values around the onset of the supercritical and the Hopf bifurcations. Stability analysis shows that, for $\alpha=-0.075$ and $k=6$, there is a loss of stability of the CCF at $r_c=0.855$ [see Fig. 3 and Eq. (26)]. Figure 8 shows the time signature, $u(t)$, and the phase trajectory in the (u,v) plane for $r=4$. The flow exhibits an oscillatory decay (from any arbitrary initial point) toward the fixed point (1.366, 0.304) in the (u,v) phase plane. As r increases, the flow remains essentially the same, with the amplitude of the steady-state solution becoming larger. At some point $r=r_0$ (in this case $r_0=6$), however, the flow undergoes a homoclinic bifurcation, as shown in Fig. 9, similarly to that predicted by the Lorenz equations [2]. In this case also, the flow decays to a fixed point $(-1.717, -0.254)$. This is a global bifurcation that cannot be detected through local stability analysis around the fixed point. What happens as r exceeds r_0 is that each unstable manifold of the origin moves from the basin of attraction of one fixed point, C_1 or C_2, to the basin of the other fixed point (for more detail on homoclinic bifurcation, refer to Ref. [35]).

At $r=r_{k1}=34.8$, linear stability analysis predicts the existence of a Hopf bifurcation, with both C_1 and C_2 losing

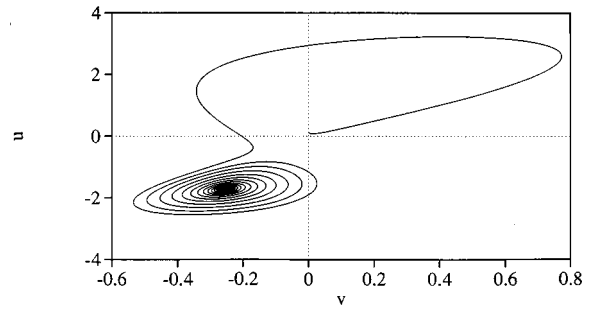

FIG. 9. Homoclinic bifurcation. Phase trajectory in the (u,v) plane for $r=6$; $\alpha=-0.075$, and $k=6$.

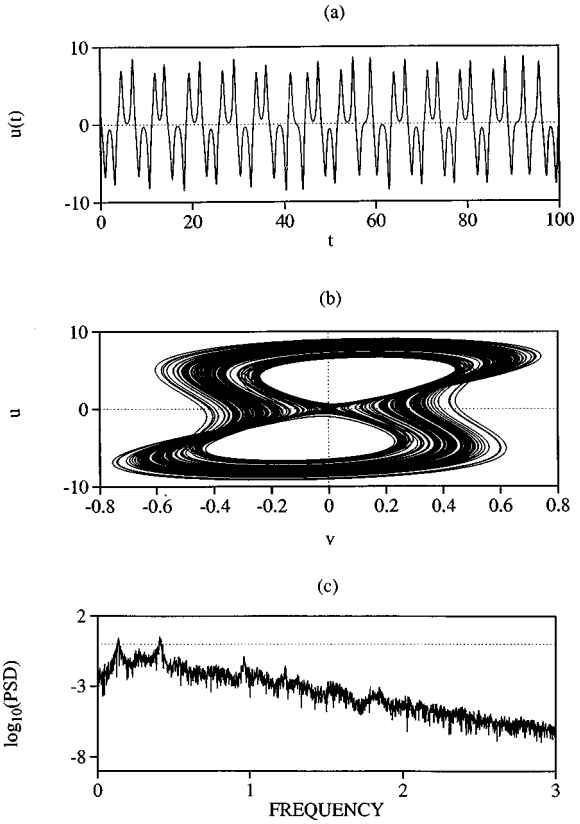

FIG. 10. Onset of aperiodic or chaotic motion for $r=35.2$, $\alpha=-0.075$, and $k=6$. Time signature $u(t)$ (a), corresponding phase trajectory in the (u,v) plane (b), and power spectrum (c).

their stability as shown in Fig. 6. At this point, the steady Taylor vortices lose their stability to adopt an oscillatory cellular structure. As r increases further, the flow becomes fully chaotic as can be seen from Fig. 10 for $r=35.2$. From the time signature [Fig. 10(a)], the phase portrait [Fig. 10(b)] and the power spectrum [Fig. 10(c)], the transition to chaos in this case appears to be similar to that leading to the Lorenz attractor. The transition does not follow any of the three well-established routes to chaos, namely, via period doubling, quasiperiodicity, or intermittency [2–4]. Finally, it is worth mentioning that (i) the exchange of stability between the CCF and the TVF via a supercritical bifurcation as r exceeds r_c, (ii) the emergence of a homoclinic bifurcation, (iii) the destabilization of the (steady) TVF through a Hopf bifurcation, and (iv) the onset of chaos, constitute a sequence of behaviors typically predicted by low-order nonlinear dynamical systems [2]. The effect of shear thinning is to lower the Taylor number for the onset of the bifurcations. The difference in dynamics will, however, become more evident as inertia is increased.

B. Flow regularization

At $r=35.9$, the flow begins to show a more coherent and even periodic behavior [see Figs. 11(a) and 11(b)]. The time signature is not shown, as it does not display any significantly new dynamics relative to Fig. 10(a). There is considerable thinning of the bandwidth of the attractor in phase space. The power spectrum in Fig. 11(b) shows a dominant frequency, $f_0=0.136$, which begins to emerge more clearly

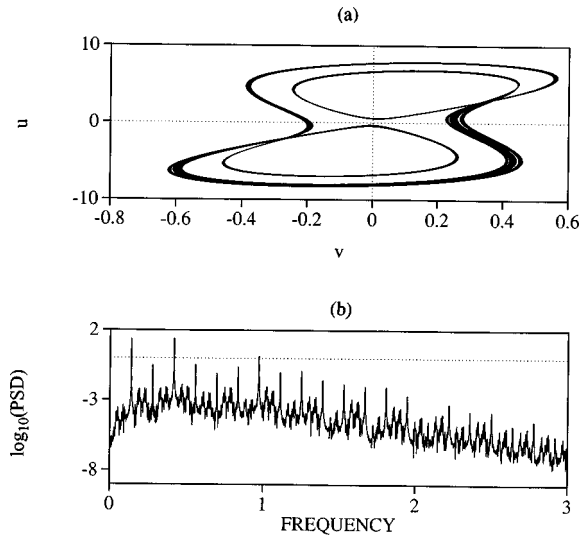

FIG. 11. Phase trajectory in the (u,v) plane (a), and power spectrum for $u(t)$ (b), for $r=35.9$, $\alpha=-0.075$, and $k=6$.

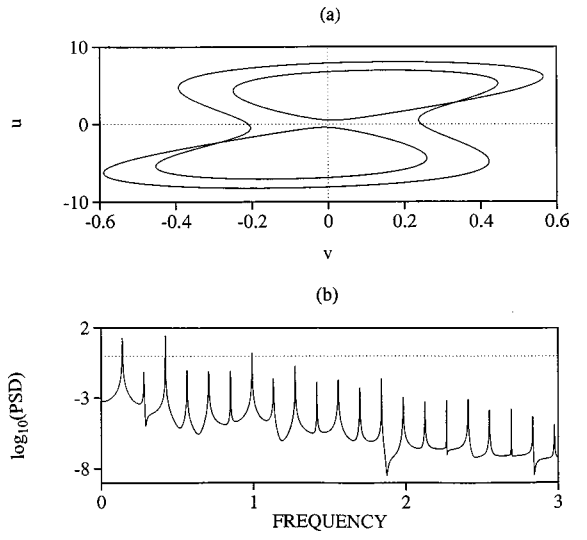

FIG. 13. Period-1 motion and even harmonics at $r=37$, $\alpha=-0.075$, and $k=6$. Phase trajectory in the (u,v) plane (a), and power spectrum for $u(t)$ (b).

than in Fig. 10(c). The spectrum shows bands of subharmonics of order 3 (multiples of $f_0/3$). The presence of subharmonics is also reflected in the phase portrait in Fig. 11(a).

The periodicity becomes more apparent for $r=36$, as shown in Fig. 12. The flow exhibits a period-2 behavior as illustrated by the phase portrait of Fig. 12(a). In the Fourier spectrum a weak subharmonic, with $f_0/2$, is identified. As r is increased, complete periodic behavior is reached, roughly at $r=37$, with the temporal behavior and phase trajectory exhibiting distortion due to nonlinear effects as shown in Fig. 13. In this case, there is no subharmonic. Merely, the even harmonics are present, which change the symmetry of $u(t)$. The basic periodic motion is shown in Fig. 14 for $r=39$. The spectrum in Fig. 14(b) contains the fundamental and its odd harmonics $(3f_0,5f_0,\ldots)$. As r increases further, the motion remains periodic with the distortion of the limit cycle slowly disappearing, and giving way to completely symmetric periodic orbits at $r=39.3$. This periodicity is, however, disrupted as r is increased further, leading to intermittent motion as discussed next.

C. Chaos via intermittency

The intermittency scenario is one of the typical routes of transition from a periodic state to chaos [2,36]. Period doubling, as discussed earlier, is another possible route. In general, a signal is called intermittent if it is subject to infrequent variations of large amplitude. Here, we are particularly interested in temporal intermittency, which can exist in dynamical systems with a small number of modes during transition from periodic to chaotic motion. The mechanisms for this phenomena were first proposed by Pomeau and Manneville [37].

For a value of r less than 39.3, the dynamical system (17) has a stable limit cycle as shown in Fig. 14; the solution oscillates in a regular fashion and is stable against small

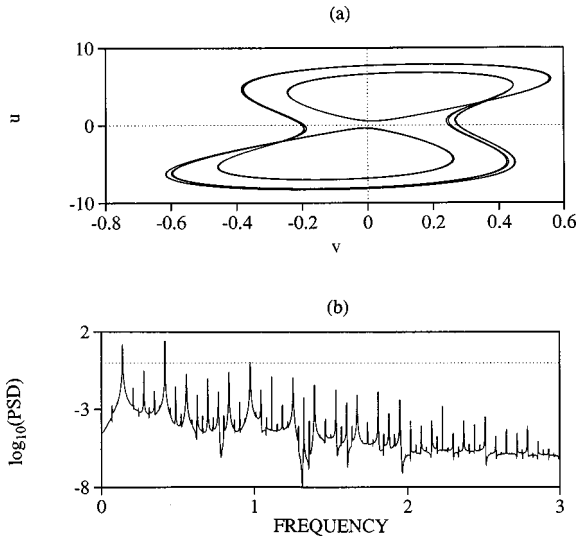

FIG. 12. Period-2 motion at $r=36$, $\alpha=-0.075$, and $k=6$. Phase trajectory in the (u,v) plane (a), and power spectrum for $u(t)$ (b).

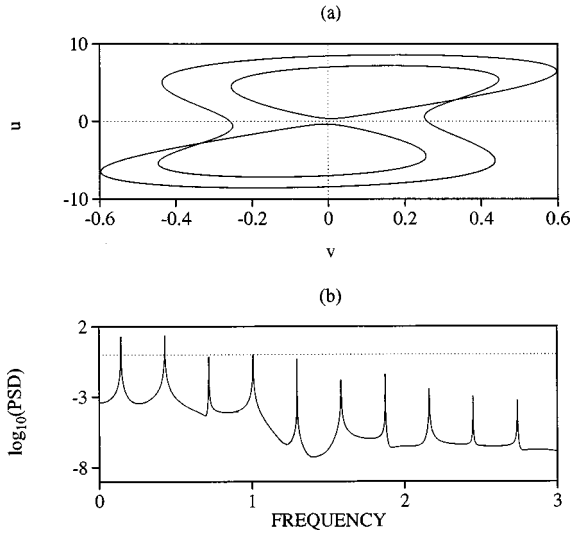

FIG. 14. Period-1 motion at $r=39$, $\alpha=-0.075$, and $k=6$. Phase trajectory in the (u,v) plane (a), and power spectrum for $u(t)$ (b).

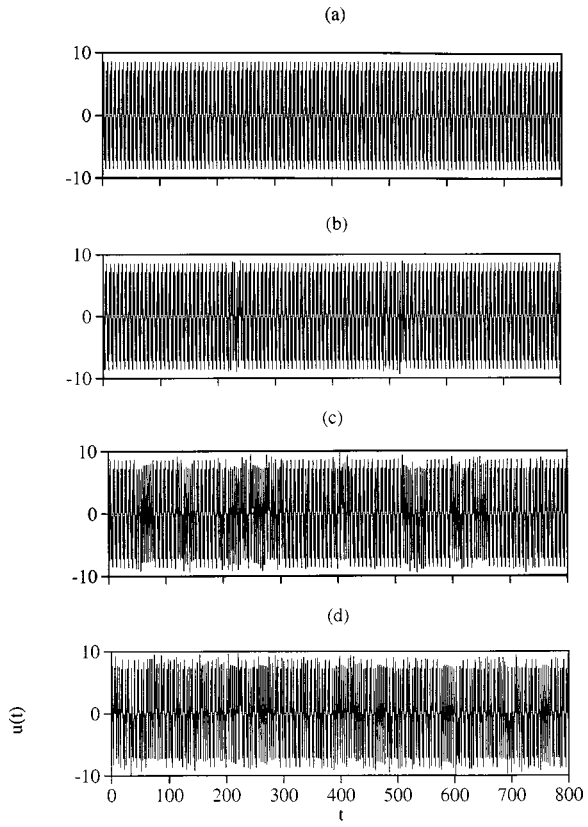

FIG. 15. Temporal behavior showing the transition to and onset of chaos via intermittency route. (a) Periodic flow at $r=39.302$, just before intermittency sets in. (b), (c) Intermittent flow at $r=39.303$ and $r=39.304$, respectively. (d) Chaos at $r=39.35$.

perturbations. When r slightly exceeds r_i (the intermittency threshold), we begin to observe an intermittent dynamical behavior, with the intermittency growing as r increases. The resulting sequence of flows is shown in Fig. 15 for $r \in [39.302, 39.350]$. It should be noted that the entire process of intermittency occurs in this narrow range of r values. The periodic behavior just before the onset of intermittency is shown in Fig. 15(a), for $r=r_i=39.302$. Intermittent flow becomes apparent at $r=39.303$ as shown in Fig. 15(b). The time signature in the figure consists of oscillations that appear regular and that resemble the stable oscillatory behavior for $r \leqslant r_i$. But now, the oscillations are interrupted from time to time by abnormal fluctuations or bursts, whose amplitude and direction are approximately the same from one fluctuation to another, and that depend on r. This is also confirmed from Fig. 15(c) at $r=39.304$, which shows that the duration of periodic behavior has decreased. Figures 15(b) and 15(c) show clearly that it is neither the amplitude nor the duration of the exceptional fluctuations that tend to increase as r increases from r_i, but only their average frequency. These erratic fluctuations have a well-defined average duration and terminate as the flow returns to the periodic oscillatory behavior. As r is further increased, the periodic flow disappears almost completely, and the motion becomes chaotic as shown in Fig. 15(d) for $r=39.35$.

V. CONCLUDING REMARKS

Although results based on low-order dynamical systems are generally interesting as they exhibit complex nonlinear flow behavior, there is always the compelling question as to their practical significance and physical relevance. To our knowledge, there is no experiment that explores directly the influence of shear thinning on the stability of TCF. In practice, it is difficult to isolate the effects of shear thinning from those of elasticity during the flow of a polymeric fluid [12,25,38,39]. However, since the present formulation is based on a truncation level similar to the one that led previously to good agreement with experiment for the TCF of non-shear-thinning viscoelastic fluids [10,40], the present results may be of practical significance. The proposed theory is not expected to be valid in the far postcritical range of Taylor numbers. It is expected to hold in the linear range, and not far beyond the critical point, i.e., after the toroidal vortex flow emerges. However, as in any approximate theory, it is often useful to probe beyond the range of validity of the model in order to stimulate future experimental and theoretical studies. More importantly, the reported formulation and results clearly show the emergence of interesting dynamics that are completely absent in the Taylor-Couette flow of Newtonian fluids, and which are solely shear-thinning induced. These dynamics are often exhibited by similar models in the thermal convection of Newtonian fluids. Thus, the approximations and assumptions made in the present formulation are expected to only shed light on the fundamental role that shear thinning plays relative to Newtonian flows.

In conclusion, the effect of shear thinning on the stability of rotating flow in the narrow-gap geometry is investigated. A low-order dynamical system is derived that generalizes Kuhlmann's system [3] that is recovered in the limit of a Newtonian fluid. The goal of the present study is to examine the impact of shear thinning on finite amplitude Taylor vortex flow. The severity of truncation involved renders the present model quite crude but allows the examination of the nonlinear range where a more realistic (numerical) approach would face difficulties. The present study elucidates the new dynamics that shear thinning generates in the nonlinear regime. From a mathematical point of view, the presence of shear thinning leads to additional cubic nonlinearities in the dynamical system, which in turn give rise to a Hopf bifurcation otherwise nonexistent in the case of a Newtonian fluid. Numerical calculations based on the current formulation show that shear thinning tends to precipitate the onset of Taylor vortices and chaos at higher Taylor numbers. The current model also predicts the complete destabilization of the Couette flow in the limit of high shear thinning, in accordance with the Rayleigh stability picture for inviscid fluids [41–43].

ACKNOWLEDGMENT

This work was supported by the Natural Sciences and Engineering Council of Canada.

APPENDIX A

The constants in Eqs. (14) are given in this Appendix:

$$A_1 = -\frac{\pi^6 + 43\pi^4 k^2 - 13\pi^2 k^4 + 9k^6}{16(\pi^2 + k^2)},$$

$$A_2=-\frac{\pi^2(\pi^4+7\pi^2k^2+k^4)}{2(\pi^2+k^2)},$$

$$A_3=2\pi^2(\pi^2-k^2),\quad A_4=-\frac{2\pi(\pi^4-6\pi^2k^2+k^4)}{(\pi^2+k^2)},$$

$$A_5=-(\pi^2+k^2), \tag{A1}$$

$$B_1=-\frac{9\pi^4+2\pi^2k^2+9k^4}{16},\quad B_2=\frac{-\pi^2(2\pi^2+k^2)}{2},$$

$$B_3=-2\pi^2(3\pi^2+k^2),\quad B_4=-2\pi(3\pi^2+k^2),$$

$$B_5=-(3\pi^2+k^2), \tag{A2}$$

$$C_1=-12\pi^4,\quad C_2=-\pi^2(3\pi^2+k^2),\quad C_3=-2\pi^4,$$

$$C_4=-\frac{\pi^2(3\pi^2+k^2)}{2},\quad C_5=\frac{\pi^3}{2},\quad C_6=-12\pi^2, \tag{A3}$$

$$D_1=-\frac{3\pi^4}{4},\quad D_2=-\frac{\pi^2(25\pi^2+3k^2)}{8},\quad D_3=-6\pi^4,$$

$$D_4=10\pi^3,\quad D_5=-3\pi^2. \tag{A4}$$

APPENDIX B

In this Appendix, the convergence of the proposed formulation is assessed. A linear stability analysis of Eqs. (11) is carried out using an arbitrary number of modes in the transverse direction (x). Equations (11) are first linearized around the origin. They reduce to the following equations:

$$u_{x,x}+u_{z,z}=0, \tag{B1}$$

$$u_{x,t}-2\tau_y(1-x)=-\rho_{,x}+(1+\alpha)(u_{x,xx}+u_{x,zz}), \tag{B2}$$

$$u_{y,t}=u_x+(1-\alpha)u_{y,xx}+(1+\alpha)u_{y,zz}), \tag{B3}$$

$$u_{z,t}=-p_{,z}+(1+\alpha)(u_{z,xx}+u_{z,zz}). \tag{B4}$$

The solution of Eqs. (B1)–(B4) is sought by using expansion (13) with $m=1$:

$$u_x(x,z,t)=\left[\sum_{n=1}^{\infty}\hat{u}_{n1}(t)\sin n\pi x\right]\cos kz, \tag{B5}$$

$$u_y(x,z,t)=\sum_{n=1}^{\infty}[\hat{v}_{n1}(t)\cos kz+\hat{v}_{n0}(t)]\sin n\pi x, \tag{B6}$$

$$u_z(x,z,t)=\left[\sum_{n=1}^{\infty}\hat{w}_{nm}(t)\cos n\pi x\right]\sin kz, \tag{B7}$$

$$p(x,z,t)=\left[\sum_{n=1}^{\infty}\hat{P}_{nm}(t)\cos n\pi x\right]\cos kz. \tag{B8}$$

Using Eqs. (B5)–(B8) and applying the Galerkin projection, the linear stability analysis leads to the following expression for the critical Taylor number, Ta_c:

$$|4\tau_n^3k^2\mathrm{Ta}_cB_{nm}-(1+\alpha)(1+\alpha+2\alpha n^2\pi^2\tau_n)\delta_{nm}|=0, \tag{B9}$$

where δ_{nm} is the Kronecker δ, $\tau_n=1/(n^2\pi^2+k^2)$, and B_{nm} is the same symmetric matrix given by Kuhlmann [3]:

$$B_{nm}=\begin{cases}1/4 & n=m\\ 0, & n-m \text{ even, nonzero}\\ \dfrac{4nm}{\pi^2(n^2-m^2)^2}, & n-m \text{ odd.}\end{cases} \tag{B10}$$

The characteristic equation (B9) yields the marginal stability curves for an arbitrary number of eigenmodes (B5)–(B8) in the (k, Ta, α) space. Note that Eq. (B9) reduces to Eq. (A4) in Ref. [3] for a Newtonian fluid, that is, as $\alpha\to 0$. Equation (B10) is solved using the IMSL-DLFDRG routine.

[1] G. R. Sell, C. Foias, and R. Temam, *Turbulence in Fluid Flows: A Dynamical Systems Approach* (Springer-Verlag, New York, 1993).
[2] P. Berge, Y. Pomeau, and C. Vidal, *Order within Chaos* (Hermann and Wiley, Paris, 1984).
[3] H. Kuhlmann, Phys. Rev. A **32**, 1703 (1985).
[4] H. Kuhlmann, D. Roth, and M. Lücke, Phys. Rev. A **39**, 745 (1988).
[5] R. E. Khayat, J. Non-Newtonian Fluid Mech. **53**, 227 (1994).
[6] R. E. Khayat, J. Non-Newtonian Fluid Mech. **58**, 331 (1995).
[7] R. E. Khayat, Phys. Rev. E **51**, 380 (1995).
[8] R. E. Khayat, J. Non-Newtonian Fluid Mech. **63**, 153 (1996).
[9] R. E. Khayat, Phys. Rev. E **51**, 2191 (1995).
[10] R. E. Khayat, Phys. Rev. Lett. **78**, 4918 (1997).
[11] R. B. Bird, R. C. Armstrong, and O. Hassager, *Dynamics of Polymeric Liquids*, 2nd ed. (Wiley, New York, 1987), Vol. 1.
[12] S. J. Muller, E. S. J. Shaqfeh, and R. G. Larson, J. Non-Newtonian Fluid Mech. **46**, 315 (1993).
[13] R. G. Larson, E. S. G. Shaqfeh, and S. J. Muller, J. Fluid Mech. **218**, 573 (1990).
[14] W. T. Ashurst and W. G. Hoover, Phys. Rev. A **11**, 658 (1975).
[15] J. J. Erpenbeck, Physica A **118**, 144 (1983).
[16] D. M. Heyes, Physica A **133**, 473 (1985).
[17] B. C. Eu, *Kinetic Theory and Irreversible Thermodynamics* (Wiley, New York, 1992).
[18] D. K. Bhattacharya and B. C. Eu, Mol. Phys. **59**, 1145 (1986).
[19] D. J. Evans, Phys. Rev. A **23**, 1988 (1981).
[20] R. E. Khayat and B. C. Eu, Phys. Rev. A **38**, 2492 (1988).
[21] R. E. Khayat and B. C. Eu, Phys. Rev. A **39**, 728 (1989).
[22] R. E. Khayat and B. C. Eu, Phys. Rev. A **40**, 946 (1989).
[23] R. E. Khayat and B. C. Eu, Rheol. Acta **30**, 204 (1991).
[24] H. Grad, Commun. Pure Appl. Math. **2**, 331 (1949).
[25] R. G. Larson, Rheol. Acta **31**, 213 (1992).
[26] G. Veronis, J. Fluid Mech. **24**, 545 (1966).
[27] H. N. Shirer and R. Wells, *Mathematical Structure of the Sin-*

gularities at the Transition Between Steady States in Hydrodynamic Systems (Springer-Verlag, Heidelberg, 1980).
[28] J. H. Curry, Commun. Math. Phys. **60**, 193 (1978).
[29] H. Yahata, Prog. Theor. Phys. **59**, 1755 (1978).
[30] H. Yahata, Prog. Theor. Phys. **61**, 791 (1979).
[31] J. A. Yorke and E. D. Yorke, in *Hydrodynamic Instabilities and the Transition to Turbulence*, edited by H. L. Swinney and J. P. Gollub (Springer-Verlag, Berlin, 1981).
[32] C. Sparrow, *The Lorenz Equations* (Springer-Verlag, New York, 1983).
[33] J. Guckenheimer and P. Holmes, *Nonlinear Oscillations, Dynamical Systems, and Bifurcations of Vector Fields* (Springer-Verlag, New York, 1983).
[34] N. Ashrafi and R. E. Khayat, Phys. Fluids (to be published).
[35] E. A. Jackson, *Perspectives of Nonlinear Dynamics* (Cambridge University, Cambridge, England, 1991), Vols. 1 and 2.
[36] H. G. Schuster, *Deterministic Chaos* (VCH Verlagsgesellschaft, Weinheim, 1995).
[37] Y. Pomeau and P. Manneville, Commun. Math. Phys. **74**, 189 (1980).
[38] R. Haas and K. Bühler, Rheol. Acta **28**, 402 (1989).
[39] B. M. Baumert and S. J. Muller, Rheol. Acta **34**, 147 (1995).
[40] R. E. Khayat, J. Fluid Mech. **400**, 33 (1999).
[41] P. G. Drazin and W. H. Reid, *Hydrodynamic Stability* (Cambridge University, Cambridge, England, 1981).
[42] R. H. Thomas and K. Walters, J. Fluid Mech. **18**, 33 (1964).
[43] M. Renardy and Y. Renardy, J. Non-Newtonian Fluid Mech. **22**, 23 (1986).